

Possible Unconventional Surface Superconductivity in the Half-Heusler YPtBi

Eylon Persky,^{1,2,3} Alan Fang,^{1,2} Xinyang Zhang,^{1,3,2} Carolina Adamo,^{1,2} Eli Levenson-Falk,^{1,3} Chandra Shekhar,⁴ Claudia Felser,⁴ Binghai Yan,⁵ and Aharon Kapitulnik^{1,2,3,6}

¹*Geballe Laboratory for Advanced Materials, Stanford University, Stanford, CA 94305, USA*

²*Stanford Institute for Materials and Energy Sciences,*

SLAC National Accelerator Laboratory, 2575 Sand Hill Road, Menlo Park, CA 94025, USA

³*Department of Applied Physics, Stanford University, Stanford, CA 94305, USA*

⁴*Max Planck Institute for Chemical Physics of Solids, 01187 Dresden, Germany.*

⁵*Department of Condensed Matter Physics, Weizmann Institute of Science, Rehovot, Israel*

⁶*Department of Physics, Stanford University, Stanford, CA 94305, USA*

(Dated: December 29, 2023)

We report an extensive study of the noncentrosymmetric half-Heusler topological superconductor YPtBi, revealing unusual relation between bulk superconductivity and the appearance of surface superconductivity at temperatures up to 3 times the bulk transition temperature. Transport measurements confirmed the low carrier density of the material and its bulk superconducting transition, which was also observed in ac susceptibility through mutual inductance (MI) measurements. However, a weak signature of superconductivity in the MI measurements appeared much above the bulk transition temperature, which was further observed in scanning tunneling spectroscopy. Polar Kerr effect measurements suggest that while the bulk superconductor may exhibit an unusual nodal superconducting state, only the surface state breaks time reversal symmetry. Complementary tunneling measurements on LuPtBi are used to establish the observations on YPtBi, while density-functional theory (DFT) calculations may shed light on the origin of this unusual surface state.

Introduction:

Topological superconductivity can be realized by inducing superconductivity at the surface of a three dimensional topological insulator (3D TI) [1]. This can be realized through interface engineering, or by using the surface states of a bulk superconductor [2–4]. These mechanisms generally lead to time-reversal invariant topological states [1], and their critical temperature is determined by that of the bulk superconductor. An alternative approach, which expands the limits of these techniques, is utilizing flat surface bands which can support superconductivity without a proximity effect. Such superconducting surface states have been observed in KZnBi [5] and t-PtBi₂ [6]. However, the topological properties of these states, particularly as related to the origin and nature of their superconducting properties, are not fully understood.

Here, we explore the possible formation of a superconducting surface state at the (111) surface of the half Heusler compound YPtBi through extensive measurements that include transport, ac susceptibility measurements through mutual inductance, scanning tunneling microscopy and spectroscopy and polar Kerr effect. While robust bulk superconductivity appears below T_c^b , we find that superconductivity at the surface persists to temperatures $T_c^s \approx 3T_c^b$. Furthermore, our Kerr effect measurements suggest that unlike the bulk, this superconducting surface state breaks time reversal symmetry (TRS), thus revealing a delicate interplay between the surface and bulk states in this paradigmatic topological system. We complement the scanning tunneling spectroscopy measurements on YPtBi with measurements LuPtBi to substantiate our arguments. To further sup-

port our experimental findings, we performed ab-initio calculations on the Bi, Lu and Pt terminations of the (111) direction, finding that a Bi-termination surface exhibits a van-Hove singularity (VHS) near the Fermi energy, which could be a source for enhanced susceptibility for a superconducting surface state. A recent theoretical study [7] explored a similar surface band structure, finding a possible domain for the onset of unconventional chiral topological surface superconductivity ahead of the bulk transition, in agreement with our results. Our results reveal a new platform for 2D chiral superconductors in which the topologically-protected surface state condense into a TRS-breaking superconducting state prior to the bulk.

In a half-Heusler compound, three metallic elements are arranged in interpenetrating fcc lattices ($C1_b$ structure) [8]. The choice of elements, with thousands of possible combinations, enables control over a wide variety of properties in the resulting compounds: structures can be metallic, semiconducting, magnetic or non-magnetic, superconducting, and they can have topological surface states [9, 10]. Of these materials, YPtBi and LuPtBi have the largest inverted gaps [11], leading to topologically protected surface states [12]. Furthermore, YPtBi and LuPtBi are bulk superconductors, with critical temperatures of 0.8 K and 1 K respectively [13, 14]. The bulk superconductivity should be a combination of odd and even parity states, due to the lack of inversion symmetry [15]. While much work was done to explore the bulk superconductivity in these materials [13, 14, 16–28], studies of surface states and their propensity to unconventional superconductivity have been limited [7].

Methods:

Single crystals of LuPtBi and YPtBi were grown by self-flux solution growth method, with Bi used as the flux medium [29–31]. The composition and structure were verified using dispersive X-ray analysis and Laue X-ray diffraction, respectively. We used X-ray Photoelectron Spectroscopy (XPS) to characterize the elemental surface composition of the samples. With a typical measurement depth of about a nanometer, pristine crystals showed traces of carbon, oxygen, and bismuth on the surface. The carbon traces were eliminated after several seconds of Ar^+ ion milling (equivalent to a few nm), and all three elements: Lu, Pt and Bi seem to appear with the correct 1:1:1 ratio, together with traces of oxygen. The surface composition did not change upon subsequent milling of several more nanometers of the surface, confirming that no other elements exist in the samples.

Resistivity and Hall effect on both types of samples, confirming the low carrier densities, $n \sim 1 \times 10^{19}/\text{cm}^3$, and relatively high mobilities, typically $\mu \sim 2500 \text{ cm}^2/\text{V-s}$ at helium temperature. Sharp bulk superconductivity was verified with both, resistive transition and two-coils mutual inductance (MI) measurements.

Scanning Tunneling Microscopy (STM) and spectroscopy (STS) measurements were performed in a modified UNISOKU Co., USM1300S $^3\text{He}^{\text{TM}}$ system with Ultra High Vacuum (UHV), 350 mK base temperature, and magnetic field capabilities. Our studies focused on samples that exhibited a clear (111) surface such as shown in the insets of Fig. 1. The data shown in this work were obtained on native as-grown surfaces without any ex-situ preparation. We performed in-situ surface cleaning by removing the top few surface layers with the STM tip itself. The details of this procedure are described in the Supplemental Material [31], and are based on a similar procedure previously used to expose superconducting regions in vacuum-cleaved YPtBi crystals [32].

High-resolution measurements of Polar Kerr Effect (PKE) were performed using a continuous wave, Zero-Area-Loop Sagnac Interferometer (ZALSI) [33, 34], in a variable temperature ^3He system. This instrument was successfully used to detect TRSB-breaking order parameters in unconventional superconductors and subtle effects of magnetism in a variety of quantum materials (see Supplemental Information [31]).

Results and Discussion:

Figure 1 shows representative base temperature (~ 350 mK) spectra of pristine surface and tip-cleaned surface for YPtBi and LuPtBi samples. While the tip-cleaned surface improved the spectra, particularly in reducing the observed zero bias conductance to very low values, the pristine surface spectra pointed to a similar large gap. At the same time the observed spectra are rounded, even well below temperatures corresponding to the observed large gap. Such a behavior could be because of nodal gap structure, high effective temperature due to RF heating or due to an intermediate thin metallic layer which depress the gap by proximity effect [35]. The fact that on

occasion we observe a flat gap as in Fig. 1b suggests that the rounding of the gap is not due to nodes in the gap.

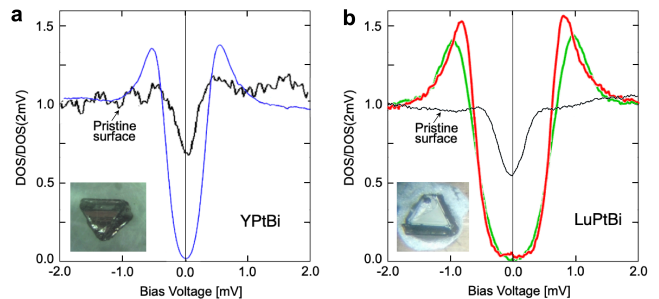


FIG. 1: Base temperature tunneling spectra. Colored spectra as example spectra after tip cleaning. a) YPtBi, b) LuPtBi. Both figures show a typical spectrum on the pristine surface, already indicating a gap much larger than the gap expected for the respective T_c s. Insets show typical crystals used in this study, both exhibit a (111) surface.

The large gaps observed at base temperature indicate that there is a superconducting system within either LuPtBi or YPtBi which involves a transition temperature higher than the bulk. Indeed, temperature dependence of tunneling spectra of both materials indicate gaps that persist much above the bulk T_c . Focusing on YPtBi, we show in Fig. 2a a typical set of spectra taken at different temperatures. Similar data on YPtBi was reported in [32]. Since the location of the coherence peaks is not a good measure of the size of the gap due to the rounded data at all temperatures, some assumptions are required to estimate the gap as a function of temperature. In a first approach we assume that “noise” interferes with the measurement and thus each spectrum is considered as a standard BCS spectrum taken at an effective temperature higher than the actual sample temperature T . Such an approach is similar to assuming an unknown broadening of the spectrum [36]. The fit to each spectrum yields the gap Δ and the effective temperature T_{eff} . Alternatively we can estimate the gap from maximum slope of the spectrum before it turns into the coherence peak (this is similar to using the maximum derivative of the spectrum [37]). Both estimates give a maximum gap of 0.4 to 0.41 meV and the fit to the BCS gap function with $2\Delta/k_B T_c = 3.52$ yields a $T_c \approx 2.85$ K.

To further investigate the onset of superconductivity, we measured the ac susceptibility of both materials using a mutual inductance technique [38]. Both materials showed a large increase of the diamagnetic response at their respective bulk transition temperatures (Figure 3), in agreement with previous reports [13, 14]. However, a careful measurement of YPtBi revealed a small increase, $\sim 0.5\%$ of the change due to the bulk transition, which onsets at ~ 3 K (Fig. 3a). This may indicate that a small volume fraction of the sample turns superconducting at a higher temperature.

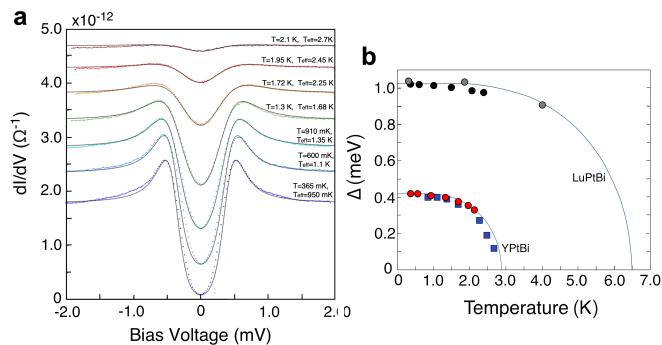


FIG. 2: Temperature dependence of tunneling spectra for YPtBi. a) a typical set of data with fits assuming noise-induced higher effective temperature (see text). b) Extracted gap as a function of temperature using two approaches: *i*) maximum slope in the gap (●) using actual measured temperature and *ii*) effective temperature higher than the actual temperature (■). Solid lines are BCS gap functions, assuming $2\Delta/k_B T_c = 3.52$. For LuPtBi (see [31]) only the maximum slope approach (●, ●) is used to determine the gap.

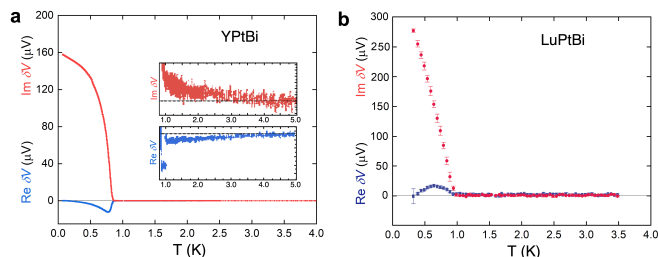


FIG. 3: Mutual inductance determination of bulk superconducting transition for (a) LuPtBi, and (b) YPtBi. Inset in (a) shows the onset of a small diamagnetic signal in YPtBi, at ~ 3 K.

The observation of a similar transition temperature for the vanishing of the superconducting gap in tunneling and a weak onset of inductive signal in mutual inductance points to an intrinsic origin of superconductivity that onsets at a temperature much above the bulk T_c^b . We envision two possible origins for the above observations. First, given our inability to make clean, atomically flat cleaves that are known to expose the (111) plane, the signals may alternatively be attributed to another compound, created during the surface cleaning, a combination of the HH elements, possibly combined with contaminants, particularly oxygen. Superconducting compounds that may be formed this way are listed in Table I. While the T_c of both amorphous and polycrystalline Bi are suitable, such compounds on the surface would generate similar transitions for both LuPtBi and YPtBi, inconsistent with the huge difference between the two compounds observed in STM measurements. We further note that LuPtBi and YPtBi are very similar chemically and

structurally (lattice constants $a = 6.58\text{\AA}$ and $a = 6.65\text{\AA}$, respectively [11]). Thus, any strained inclusion of a different compound on the surface would be expected to yield a similar gap. Moreover, the similarity in the behavior of LuBi and YBi may rule this possibility out as well, particularly since they require pressure to exhibit superconductivity.

Compound	Bi	a-Bi	p-Bi	BiPt	Bi ₂ Pt	YBi	LuBi
P (GPa)	amb.	amb.	amb.	amb.	5-6	$\gtrsim 2.6$	$\gtrsim 3$
T_c (K)	$\ll 0.1^1$	$5-6^2$	6.1^3	1.3^4	$\sim 2^5$	$\sim 5^6$	$4-7.5^7$

TABLE I: Possible superconducting compounds derived from YPtBi and LuPtBi. While “amb.” represents ambient pressure, some compounds only become superconducting at a finite pressure. Source references: ¹[39], ²[40], ³[41, 42], ⁴[43], ⁵[44], ⁶[45], ⁷[46].

The alternative explanation for the observed higher T_c in the two compounds is the creation of a chiral surface state. Particularly, since both LuPtBi and YPtBi are known to be topological with a large band inversion [11], it was suggested that superconductivity associated with this material is topological and may break TRS [22, 23]. To test this possibility, particularly for YPtBi, we performed high resolution polar Kerr effect measurements using a zero-area-loop Sagnac interferometer (ZALSI) [33, 34]. By construction, the ZALSI is inherently reciprocal and thus by its symmetry it can distinguish between true TRSB Kerr effect and optical activity when reflected from a chiral medium. In our implementation we use two orthogonally counter propagating linearly polarized light beams, which are then converted into right and left circular polarizations using a quarter-wave plate. An objective lens focuses the light onto a small interaction region on the sample, and the reflected light beams are converted back to linear polarizations with exchanged polarization directions. Owing to the reciprocity of the apparatus, any non reciprocal phase shift $\phi_{nr} = 2\theta_K$ will appear at the detector only if TRS is broken through the interaction of the two circularly polarized beams with the sample [33, 34] (see supplementary material [31]).

We cooled down the sample to ~ 300 mK from a high temperature in the presence of a small external magnetic field, and then removed the field and measured the Kerr signal while warming up the sample (Figure 4a). For small training fields ($H \lesssim 50$ Oe) the initial signal (at 300 mK) following the removal of the magnetic field was very small, consistent with zero (within our resolution of $\sim 0.05 \mu\text{rad}$). However, increasing the temperature from base temperature, a finite Kerr signal of order $\pm 0.25 \mu\text{rad}$ appeared above the bulk T_c^b . The signal was independent of the field strength and changed sign upon changing the direction of the training field (Figure 4b). These features indicate a TRS breaking state, and are generally similar to those observed in chiral superconductors [47, 48].

With strong structural and electronic structure similarities to GdPtBi, we estimate the optical penetration

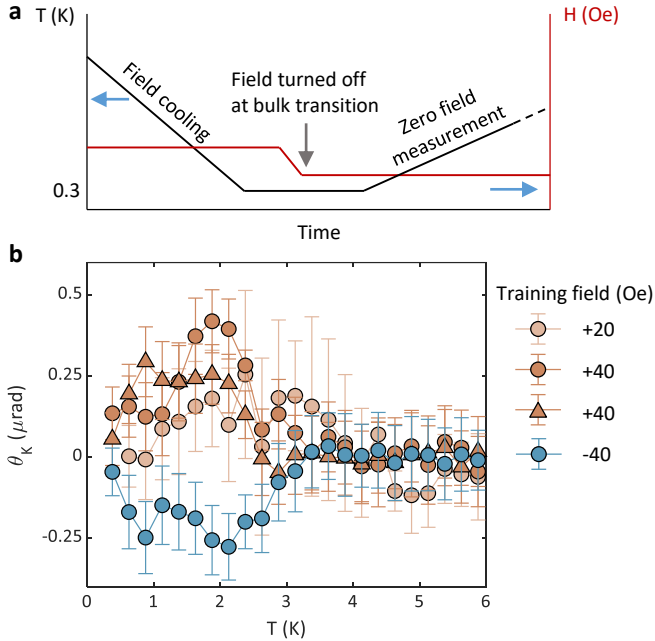


FIG. 4: Polar Kerr effect measurements on a (111) face of a pristine YPtBi crystal. (a) The sample was first cooled in a magnetic field to base temperature (~ 300 mK). The field was then removed, and Kerr data was taken while warming up the sample. (b) The resulting Kerr signals for various low training fields. A finite Kerr signal appears much above the bulk T_c^b of the sample. The error bars represent a 95% confidence interval, based on statistical averaging within each temperature bin.

depth of YPtBi at ~ 150 nm [49]. Thus, the Kerr signal can have both bulk and surface contributions. In particular above the bulk T_c^b the observed Kerr signal may be a result of TRS breaking associated with the surface superconductivity - a favorable possibility since Kerr effect persists very close to the surface T_c^s , or it may be associated with vestigial order [50] originating from the bulk superconducting state. However, the fact that Kerr effect is observed up to three times the bulk T_c^b makes the vestigial order possibility unlikely.

While low field training (i.e. training in $H \lesssim 50$ Oe) yields similar onset and size of Kerr signal, which follows the direction of the training field, cooling the sample at higher magnetic field to base temperature (0.3 K), turning the field to zero and measuring while warming up the sample in zero magnetic field yields a signal that is zero within our resolution of ~ 0.05 μrad . However, cooling the sample at higher magnetic field to base temperature (0.3 K), but on the way turning the magnetic field to zero at $T \approx 1.3$ K, then measuring the Kerr effect at zero field from base temperature up yields results similar to the low field training experiments. Fig. 5 summarizes these findings.

Such a peculiar effect may point to a delicate interplay

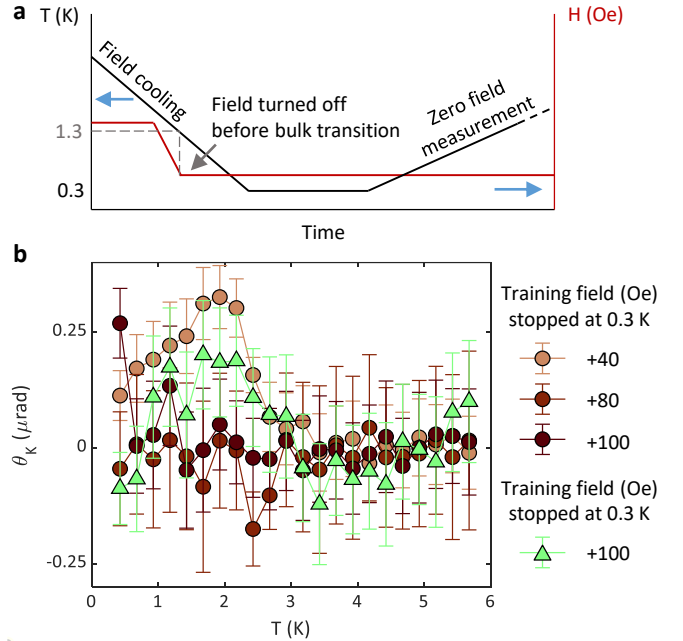


FIG. 5: Polar Kerr effect after higher-field training. (a) An alternative training protocol, where the magnetic field was removed at 1.3 K, before the bulk superconducting transition. (b) The Kerr signals obtained after training at low and high fields (> 80 Oe) with the original training protocol, and after high-field training with the new protocol. Note that θ_K is suppressed or reversed when trained at a high field. However, the sample could be trained even when the field was switched off before the bulk transition, and the original sign of θ_K was recovered.

between the vortex state that appears in the bulk material upon cooling in a field much below the bulk T_c^b and the effect on the surface state. For example, cooling at lower field and removing the field at low temperatures may result in low vortex occupancy due to weak surface and geometrical barriers (note that $H_{c1} \lesssim 3$ Oe, while the thermodynamic critical field is $H_{c1} \lesssim 100$ Oe for the bulk superconducting state of these materials). Above a field of order $\gtrsim 100$ Oe, enough vortices may remain in the bulk, which upon crossing the bulk T_c will move out of the sample, thus possibly “scrambling” the single domain nature of the TRS-breaking state of the surface superconductivity. We note that the apparent suppression of the Kerr effect at temperatures below T_c^b suggests points to a TRS-preserving bulk superconducting state. This is consistent with the observations of nodes in the bulk and the analysis of the possible spin and orbital pairing states [23]. Thus, the magnetization of the surface state interacts with a conventional superconducting order parameter. This is similar to magnetic superconductors, where the formation and motion of vortices can change the ferromagnetic order parameter [51].

Taken together, the STM, mutual inductance and PKE

results indicate that the (111) surfaces of YPtBi and LuPtBi host a superconducting state which breaks TRS. To understand the origin of this state, we studied the surface band structure of LuPtBi (see Supplementary Information [31]). In Bi-terminated (111) surfaces, we found a van-Hove singularity close to the M -point, giving rise to an enhanced density of states near the Fermi level. This could be the driving force behind the enhanced surface T_c^s . The calculated band structure of the Lu terminated surface, did not show van-Hove singularities. Schwemmer *et al.* [7] have recently reported a detailed study of the surface band structure and possible superconductivity of the Bi-terminated (111) surface of LuPtBi. While the gross features of their surface band structure are similar to our calculation, they also revealed flat-band regions near the Fermi energy, and calculated propensity to a superconducting instability. In particular, they argue that the transition temperature of the surface state is independent of the bulk transition, and exhibit vestigial time-reversal symmetry breaking in its fluctuation regime. Since inversion symmetry is broken, simple singlet and/or triplet states were dismissed and pairing was tested for pairs of electrons that are connected by the TR operator. The result has been a pair-amplitude that transforms under the E irreducible representation of the surface's C_{3v} point group (relevant to the (111) crystal orientation) in the presence of strong Kane-Mele type and Rashba type spin-orbit coupling [52]. Furthermore, they found that a chiral superconducting state, which spontaneously breaks TRS, is energetically favorable.

In conclusion, we presented above a comprehensive study of scanning tunneling spectroscopy of the tip-

cleaned (111) surface of the half-Heusler alloys YPtBi and LuPtBi. While a bulk T_c^b of ~ 0.8 K is observed for both systems, we find a much larger corresponding gap in our tunneling studies with T_c^s 's of ~ 2.3 K and ~ 6.5 K for YPtBi and LuPtBi respectively. Mutual inductance measurements of YPtBi further revealed a small diamagnetic response that onsets around T_c^s . Polar Kerr effect on YPtBi indicate that TRS is broken near or at T_c^s . Together, our data indicate that chiral surface superconductivity may precede bulk condensation in these materials, a hypothesis which is strongly supported by recent calculations [7]. While additional work is required to determine the order parameter of these states, our results open a new direction to engineering topological superconducting states in half Heusler compounds. While our study was conducted on single crystals, Kim *et al.* [53] recently demonstrated epitaxially growth of YPtBi films, which can also be encapsulated by an alumina film, preventing degradation of the surface. This system is therefore highly promising for quantum device applications.

ACKNOWLEDGMENTS

We thank Ronny Thomale and Jörg Schmalian for illuminating discussions. This work was supported by the U. S. Department of Energy (DOE) Office of Basic Energy Science, Division of Materials Science and Engineering at Stanford under contract No. DE-AC02-76SF00515. EP was partially supported by the Koret Foundation.

-
- [1] L. Fu, and C. L. Kane, "Superconducting Proximity Effect and Majorana Fermions at the Surface of a Topological Insulator," *Phys. Rev. Lett.* 100, 096407 (2008)
 - [2] A.K. Nayak, A. Steinbok, Y. Roet, J. Koo, G. Margalit, I. Feldman, A. Almoalem, A. Kanigel, G. Fiete, B. Yan, Y. Oreg, N. Avraham and H. Beidenopf, "Evidence of topological boundary modes with topological nodal-point superconductivity," *Nat. Phys.* 17, 1413–1419 (2021).
 - [3] O.J. Clark, M.J. Neat, K. Okawa, L. Bawden, I. Marković, F. Mazzola, J. Feng, V. Sunko, J.M. Riley, W. Meevasana, J. Fujii, I. Vobornik, T.K. Kim, M. Hoesch, T. Sasagawa, P. Wahl, M.S. Bahramy, and P.D.C. King, "Fermiology and Superconductivity of Topological Surface States in PdTe₂," *Phys. Rev. Lett.* 120, 156401 (2018).
 - [4] P. Zhang, K. Yaji, T. Hashimoto, Y. Ota, T. Kondo, K. Okazani, Z. Wang, J. Wen, G.D. GU, H. Ding, and S. Shin, "Observation of topological superconductivity on the surface of an iron-based superconductor," *Science* 360, 182-186 (2018).
 - [5] J. Song, S. Kim, Y. Kim, H. Fu, J. Koo, Z. Wang, G. Lee, J. Lee, S.H. Oh, J. Bang, T. Matsushita, N. Wada, H. Ikegami, J.D. Denlinger, Y.H. Lee, B. Yan, Y. Kim, and S.W. Kim, "Coexistence of Surface Superconducting and Three-Dimensional Topological Dirac States in Semimetal KZnBi," *Phys. Rev. X* 11, 021065 (2021).
 - [6] Sebastian Schimmel, Yanina Fasano, Sven Hoffmann, Joaquín Puig, Grigory Shipunov, Danny Baumann, Saicharan Aswartham, Bernd Büchner, and Christian Hess, "High- T_C surface superconductivity in topological Weyl semimetal t-PtBi₂," arXiv:2302.08968 [cond-mat.supr-con] (2023).
 - [7] Tilman Schwemmer, Domenico Di Sante, Jörg Schmalian, Ronny Thomale, "Chiral surface superconductivity in half-Heusler semimetals," arXiv:2212.09786 [cond-mat.supr-con] (2022).
 - [8] Tanja Graf, Claudia Felser, and Stuart S.P. Parkin, "Simple rules for the understanding of Heusler compounds," *Prog. Solid. State Ch.* 39, 1-50 (2011).
 - [9] Kaustuv Manna, Yan Sun, Lukas Muechler, Jürgen Kübler, and Claudia Felser, "Heusler, Weyl and Berry," *Nat Rev Mater* 3, 244–256 (2018).
 - [10] Sheron Tavares, Kesong Yang, and Marc A. Meyers, "Heusler alloys: Past, properties, new alloys, and prospects," *Prog. Mater. Sci.* 132, 101017 (2023).
 - [11] S. Chadov, X. L. Qi, J. Kübler, G. H. Fecher, C. Felser, and S. C. Zhang, "Tunable multifunctional topological insulators in ternary Heusler compounds," *Nat. Mater.*

- 9, 541 (2010).
- [12] Z. K. Liu, L. X. Yang, S.-C. Wu, C. Shekhar, J. Jiang, H. F. Yang, Y. Zhang, S.-K. Mo, Z. Hussain, B. Yan, C. Felser, and Y. L. Chen, “Observation of unusual topological surface states in half-Heusler compounds LnPtBi ($\text{Ln}=\text{Lu}, \text{Y}$),” *Nat. Commun* 7, 12924 (2016).
- [13] N. P. Butch, P. Syers, K. Kirshenbaum, A. P. Hope, and J. Paglione, “Superconductivity in the topological semimetal YPtBi ,” *Phys. Rev. B* 84, 220504 (2011).
- [14] F. F. Tafti, Takenori Fujii, A. Juneau-Fecteau, S. René de Cotret, N. Doiron-Leyraud, Atsushi Asamitsu, and Louis Taillefer, “Superconductivity in the noncentrosymmetric half-Heusler compound LuPtBi : A candidate for topological superconductivity,” *Phys. Rev. B* 87, 184504 (2013).
- [15] M. Smidman, M. B. Salamon, H. Q. Yuan, and D. F. Agterberg, “Superconductivity and spin-orbit coupling in non-centrosymmetric materials: a review,” *Rep. Prog. Phys.* 80, 036501 (2017).
- [16] T. V. Bay, T. Naka, Y. K. Huang, and A. de Visser, “Superconductivity in noncentrosymmetric YPtBi under pressure,” *Phys. Rev. B* 86, 064515 (2012).
- [17] T.V. Bay, M. Jackson, C. Paulsen, C. Baines, A. Amato, T. Orvis, M.C. Aronson, Y.K. Huang, A. de Visser, “Low field magnetic response of the non-centrosymmetric superconductor YPtBi ,” *Solid State Comm.* 183, 13 (2014).
- [18] Markus Meinert, “Unconventional Superconductivity in YPtBi and Related Topological Semimetals,” *Phys. Rev. Lett.* 116, 137001 (2016).
- [19] Orest Pavlosiuk, Dariusz Kaczorowski, and Piotr Wiśniewski, “Superconductivity and Shubnikov-de Haas oscillations in the noncentrosymmetric half-Heusler compound YPtBi ,” *Phys. Rev. B* 94, 035130 (2016).
- [20] C. Timm, A. P. Schnyder, D. F. Agterberg, and P. M. R. Brydon, “Inflated nodes and surface states in superconducting half-Heusler compounds,” *Phys. Rev. B* 96, 094526 (2017).
- [21] Hao Yang, Jiabin Yu, Stuart S.P. Parkin, Claudia Felser, Chao Xing Liu, and Binghai Yan, “Prediction of Triple Point Fermions in Simple Half-Heusler Topological Insulators,” *Phys. Rev. Lett.* 119, 136401 (2017).
- [22] Lucile Savary, Jonathan Ruhman, Jörn W. F. Venderbos, Liang Fu, and Patrick A. Lee, “Superconductivity in three-dimensional spin-orbit coupled semimetals,” *Phys. Rev. B* 96, 214514 (2017).
- [23] Hyunsoo Kim, Kefeng Wang, Yasuyuki Nakajima, Rongwei Hu, Steven Ziemak, Paul Syers, Limin Wang, Halyna Hodovanets, Jonathan D. Denlinger, Philip M. R. Brydon, Daniel F. Agterberg, Makariy A. Tanatar, Ruslan Prozorov, Johnpierre Paglione, “Beyond triplet: Unconventional superconductivity in a spin-3/2 topological semimetal,” *Sci. Adv.* 4, eaao4513 (2018).
- [24] Jörn W.F. Venderbos, Lucile Savary, Jonathan Ruhman, Patrick A. Lee, and Liang Fu, “Pairing States of Spin-3/2 Fermions: Symmetry-Enforced Topological Gap Functions,” *Phys. Rev. X* 8, 011029 (2018).
- [25] Qing-Ze Wang, Jiabin Yu, and Chao-Xing Liu, “Unconventional superconductivity and surface pairing symmetry in half-Heusler compounds,” *Phys. Rev. B* 97, 224507 (2018).
- [26] Bitan Roy, Sayed Ali Akbar Ghorashi, Matthew S. Foster, and Andriy H. Nevidomskyy, “Topological superconductivity of spin-3/2 carriers in a three-dimensional doped Luttinger semimetal,” *Phys. Rev. B* 99, 054505 (2019).
- [27] Hyunsoo Kim, Makariy A. Tanatar, Halyna Hodovanets, Kefeng Wang, Johnpierre Paglione, and Ruslan Prozorov, “Campbell penetration depth in low carrier density superconductor YPtBi ,” *Phys. Rev. B* 104, 014510 (2021).
- [28] Hyunsoo Kim, Junhyun Lee, Halyna Hodovanets, Kefeng Wang, Jay D. Sau, and Johnpierre Paglione, “Quantum oscillations of the $j = 3/2$ Fermi surface in the topological semimetal YPtBi ,” *Phys. Rev. Research* 4, 033169 (2022).
- [29] P. C. Canfield, J. D. Thompson, W. P. Beyermann, A. Lacerda, M. F. Hundley, E. Peterson, Z. Fisk, and H. R. Ott, “Magnetism and heavy fermion-like behavior in the RBiPt series,” *J. Appl. Phys.* 70, 5800 (1991).
- [30] P. C. Canfield and Z. Fisk, “Growth of single crystals from metallic fluxes,” *Philos. Mag.* B 65, 1117 (1992).
- [31] Supplemental Information - URL to be determined by publisher.
- [32] Hongwoo Baek, Jeonghoon Ha, Duming Zhang, Bharath Natarajan, Jonathan P. Winterstein, Renu Sharma, Rongwei Hu, Kefeng Wang, Steven Ziemak, Johnpierre Paglione, Young Kuk, Nikolai B. Zhitenev, and Joseph A. Stroscio, “Creating nanostructured superconductors on demand by local current annealing,” *Phys. Rev. B* 92, 094510 (2015).
- [33] Jing Xia, Peter T. Beyersdorf, Martin M. Fejer, Aharon Kapitulnik, “Modified Sagnac interferometer for high-sensitivity magneto-optic measurements at cryogenic temperatures,” *Applied Physics Letters* 89, 062508 (2006).
- [34] Aharon Kapitulnik, Jing Xia, Elizabeth Schemm and Alexander Palevski, “Polar Kerr effect as probe for time-reversal symmetry breaking in unconventional superconductors,” *New J. Phys.* 11, 055060 (2009).
- [35] N. Moussy, H. Courtois, and B. Pannetier, “Local spectroscopy of a proximity superconductor at very low temperature,” *Europhys. Lett.*, 55, 861 (2001).
- [36] R. C. Dynes, V. Narayanamurti, and J. P. Garno, “Direct Measurement of Quasiparticle-Lifetime Broadening in a Strong-Coupled Superconductor,” *Phys. Rev. Lett.* 41, 1509 (1978).
- [37] Toshiyuki Kita, Daisuke Akasako, Hironaru Murakami and Ryoza Aoki, “Gap Value Determinations on the Tunneling Spectrum,” in *Advances in Superconductivity VII*, K. Yamafuji et al. (eds.), (Springer-Verlag Tokyo 1995.)
- [38] Xinyang Zhang, Mark Zic, Dong Chen, Chandra Shekhar, Claudia Felser, Ian R. Fisher, and Aharon Kapitulnik, “Vortex phase diagram of kagome superconductor CsV_3Sb_5 ,” *arXiv:2306.13297 [cond-mat.supr-con]* (2023).
- [39] O. Prakash, A. Kumar, A. Thamizhavel, S. Ramakrishnan, “Evidence for bulk superconductivity in pure bismuth single crystals at ambient pressure,” *Science* 355, 52 (2017).
- [40] J. T. Chen, T. T. Chen, J. D. Leslie and H. J. T. Smith, “Strong-Coupling Superconductivity in Amorphous Bismuth,” *Physics Letters A* 25, 679 (1967).
- [41] V. I. Petrosyan, V. N. Molin, O. I. Vasin, P. A. Skripkina, S. I. Stenin, and E. G. Batyev, “Superconductivity in polycrystalline bismuth films,” *Zh. Eksp. Teor. Fiz.* 66, 995-100 (1974).
- [42] Mingliang Tian, Jinguo Wang, Nitesh Kumar, Tianheng Han, Yoji Kobayashi, Ying Liu, Thomas E. Mallouk, and

- Moses H. W. Chan, "Observation of Superconductivity in Granular Bi Nanowires Fabricated by Electrodeposition," *Nano Letters* 6, 2773 (2006).
- [43] N.N. Zhuravlev, A.A. Stepanova, N.I. Zyuzin, "On the Superconductivity of the Compound BiPt," *J. Exptl. Theoret. Phys. (U.S.S.R.)* 37, 880-881 (1959).
- [44] Jing Wang, Xuliang Chen, Yonghui Zhou, Chao An, Ying Zhou, Chuanchuan Gu, Mingliang Tian, and Zhaorong Yang, "Pressure-induced superconductivity in trigonal layered PtBi₂ with triply degenerate point fermions," *Phys. Rev. B* 103, 014507 (2021).
- [45] C. Q. Xu, B. Li, M. R. van Delft, W. H. Jiao, W. Zhou, B. Qian, Nikolai D. Zhigadlo, Dong Qian, R. Sankar, N. E. Hussey, and Xiaofeng Xu, "Extreme magnetoresistance and pressure-induced superconductivity in the topological semimetal candidate YBi," *Phys. Rev. B* 99, 024110 (2019).
- [46] H. Gu, F. Tang, Y.-R. Ruan, J.-M. Zhang, R.-J. Tang, W. Zhao, R. Zhao, L. Zhang, Z.-D. Han, B. Qian, X.-F. Jiang, and Y. Fang, "Pressure effect on the topologically nontrivial electronic state and transport of lutetium monobismuthide," *Phys. Rev. Materials* 4, 124204 (2020).
- [47] E. R. Schemm, W. J. Gannon, C. M. Wishne, W. P. Halperin, and A. Kapitulnik, "Observation of broken time-reversal symmetry in the heavy-fermion superconductor UPt₃," *Science* 345, 190-193 (2014).
- [48] I. M. Hayes, D. S. Wei, T. Metz, J. Zhang, Y. S. Eo, S. Ran, S. R. Saha, J. Collini, N. P. Butch, D. F. Agterberg, A. Kapitulnik, and J. Paglione, "Multicomponent superconducting order parameter in UTe₂," *Science* 373, 797-801 (2021).
- [49] F. Hütt, A. Yaresko, M. B. Schilling, C. Shekhar, C. Felser, M. Dressel, and A. V. Pronin, "Linear-in-Frequency Optical Conductivity in GdPtBi due to Transitions near the Triple Points," *Phys. Rev. Lett.* 121, 176601 (2018).
- [50] Rafael M. Fernandes, Peter P. Orth, and Jörg Schmalian, "Intertwined Vestigial Order in Quantum Materials: Nematicity and Beyond," *Annual Review of Condensed Matter Physics* 10, 133 (2019).
- [51] C. Paulsen, D. J. Hykel, K. Hasselbach, and D. Aoki, "Observation of the Meissner-Ochsenfeld Effect and the Absence of the Meissner State in UCoGe," *Phys. Rev. Lett.* 109, 237001 (2012).
- [52] Manuel Laubach, Johannes Reuther, Ronny Thomale, and Stephan Rachel, "Rashba spin-orbit coupling in the Kane-Mele-Hubbard model," *Phys. Rev. B* 90, 165136 (2014).
- [53] Jiwoong Kim, Kajetan M. Fijalkowski, Johannes Kleinlein, Claus Schumacher, Anastasios Markou, Charles Gould, Steffen Schreyeck, Claudia Felser, and Laurens W. Molenkamp, "Molecular beam epitaxy of a half-Heusler topological superconductor candidate YPtBi," *Phys. Rev. Materials* 7, 024802 (2023).
- [54] G. Kresse and J. Hafner, "Ab initio molecular dynamics for liquid metals," *Phys. Rev. B* 47, 558(R) (1993).

SUPPLEMENTAL INFORMATION

Possible Unconventional Surface Superconductivity in the Half-Heuslers LuPtBi and YPtBi

Eylon A. Persky^{1,2,3}, Alan Fang,^{1,2} Carolina Adamo,^{1,2} Eli Levenson-Falk,^{1,3} Qi I. Yang,^{1,4} Chandra Shekhar,⁵ Claudia Felser,⁵ Binghai Yan,⁶ and Aharon Kapitulnik^{1,2,3,4}

¹*Geballe Laboratory for Advanced Materials, Stanford University, Stanford, California 94305, USA*

²*Stanford Institute for Materials and Energy Sciences, SLAC National Accelerator Laboratory, 2575 Sand Hill Road, Menlo Park, California 94025, USA*

³*Department of Applied Physics, Stanford University, Stanford, California 94305, USA*

⁴*Department of Physics, Stanford University, Stanford, California 94305, USA*

⁵*Max Planck Institute for Chemical Physics of Solids, 01187 Dresden, Germany.*

⁶*Department of Condensed Matter Physics, Weizmann Institute of Science, Rehovot, Israel*

S1. CRYSTAL GROWTH AND SAMPLE FABRICATION

Single crystals of YPtBi and LuPtBi were grown by self-flux solution growth method, whereas Bi provides a flux medium. For example, the stoichiometry quantities of freshly polished piece of elements Lu, Pt and Bi of purity $> 99.99\%$ in the 0.3:0.3:10 atomic ratio were put in tantalum crucible and sealed in dry quartz ampoule under 3 mbar partial pressure of argon. The mixture containing ampoule was heated at a rate of 100 K/h up to 1473 K and followed by 12 hours soaking. For crystal growth, the temperature was slowly reduced by 2 K/h to 873 K and removed extra Bi flux by decanting the ampoule at 873 K. In this method, we get 2-3 mm regular triangle size of crystals, and their preferred growth orientation is (111), which was confirmed by Laue diffraction. The general method of crystals growth has been followed from literatures [29, 30]. The composition and structure were checked by energy dispersive X-ray analysis and Laue X-ray diffraction, respectively. The lattice parameters of the cubic structure are 6.574, which are consistent with previous reports [11, 14]. Energy dispersive x-ray spectrometry gives atomic percentages 33.6: 33.0: 33.4 \pm 3.0 % for Lu: Pt: Bi confirming the stoichiometric ratio of the chemical compositions. Similar procedure and results were obtained for YPtBi.

S2. SURFACE PROPERTIES AND MORPHOLOGY

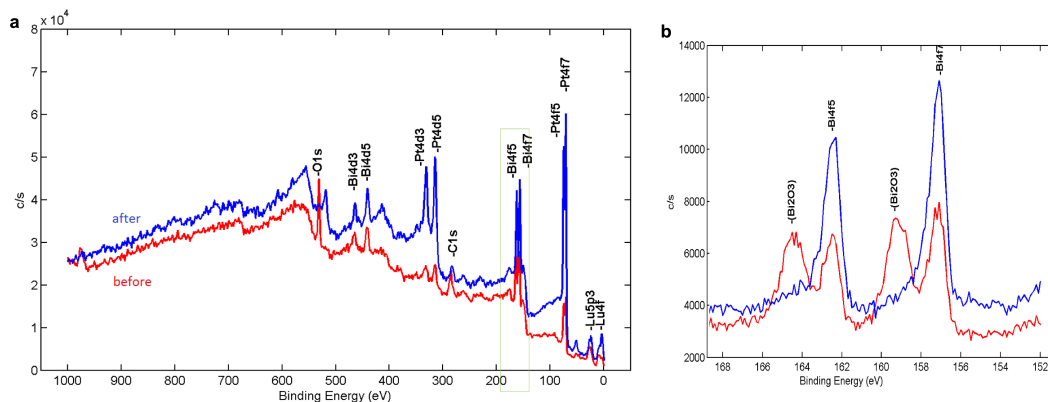


FIG. S1: XPS studies of a LuPtBi crystal before and after ion milling. We also show an expanded region around 160 eV, showing the removal of bismuth-oxide and strengthening the LuPtBi-bonded bismuth.

To understand the morphology and chemistry of the surface of the crystals we used X-ray Photoelectron Spectroscopy (XPS) that allows for high sensitivity elemental surface composition measurement and high resolution binding energy chemical shift measurement of solid samples under high vacuum. With typical measurement depth of about a nanometer, pristine crystals show traces of carbon, oxygen, and bismuth on the surface. However, after a several seconds of ion milling (equivalent to a few nm), all carbon traces are gone and all three elements: Lu, Pt and Bi seem to appear with the correct 1:1:1 ratio, together with traces of oxygen. This results does not change after subsequent milling of several more nanometers of the surface, confirming that no other elements exist in the samples.

S3. SURFACE CLEANING PROCEDURE USING STM TIP

The ease by which the fresh surface oxidizes suggests that ex-situ milling and then loading the sample into the STM may not solve the surface contamination problem. To overcome this issue, we performed in-situ surface cleaning by using the STM itself to remove the top few layers and expose deeper layers, presumably reaching the true surface layer of the crystal. In a typical conditions of this process, performed in-situ at helium temperature under UHV conditions, the STM tip junction resistance was set by a bias of 20-50 mV and current of 100 pA. Then voltage pulses of a few volts were applied until zero bias conductance was minimized. Occasionally, we found regions of area of $\sim 5 \times 5 \text{ nm}^2$, which were flat and untilted to within a few angstroms, yet had an indistinct but reproducible topography (no atomic corrugations above 10's of pm were seen, most likely due to tip bluntness). Since we focused on the temperature range below T_c^b , the quality of spectra were gauged by how close the DOS reached zero at zero bias, as expected for gapped spectra. A similar method was previously used to expose superconducting regions in vacuum-cleaved YPtBi crystals by Baek *et al.* [32], although no particular effort was made to study the topological (111) direction of the crystals. Notably our (111) starting surface, while showing “lumpy” topography similar to [32], was overall much flatter, with only $\sim 0.3 \text{ nm}$ height variations over 50 nm regions (as opposed to $\sim 1 \text{ nm}$ in [32]).

S4. STM MEASUREMENTS

As noted in the main text, we performed measurements on a modified UNISOKU Co., USM1300S³HeTM system with Ultra High Vacuum (UHV), 350 mK base temperature, and magnetic field capabilities.

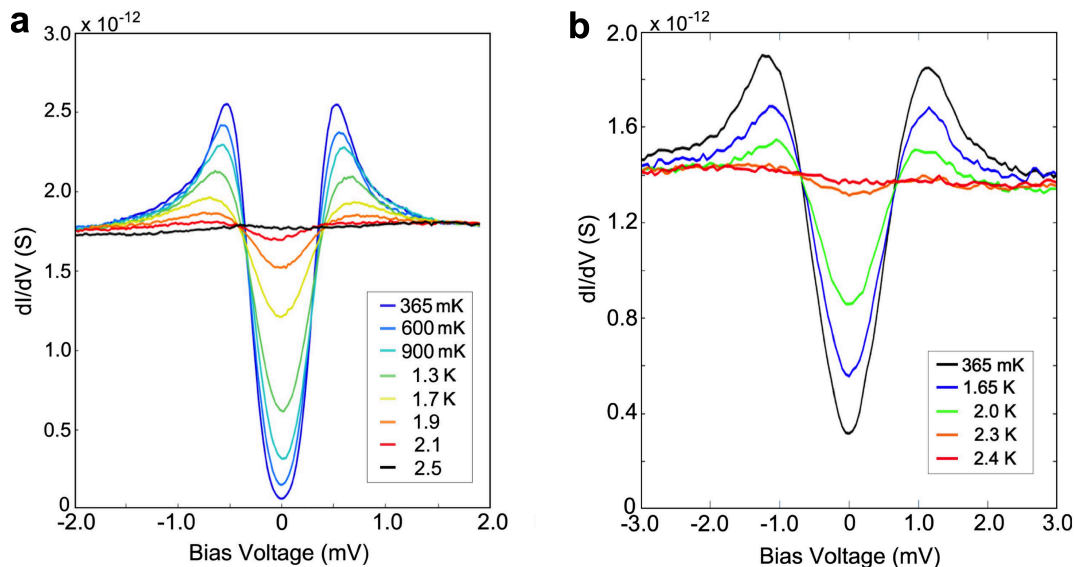


FIG. S2: Examples of surface spectroscopy following tip-cleaning procedure as a function of temperature for a) YPtBi and b) LuPtBi.

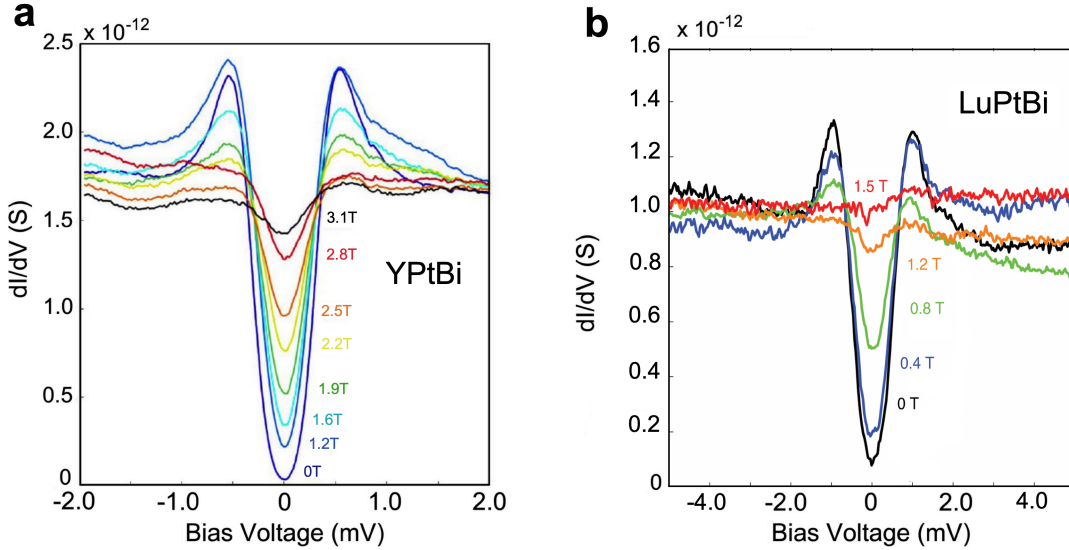


FIG. S3: Examples of surface spectroscopy following tip-cleaning procedure performed at base temperature (365 mK) as a function of magnetic field for a) YPtBi and b) LuPtBi.

S5. KERR EFFECT MEASUREMENTS

High-resolution measurements of Kerr rotation were performed using a fiber-based zero-area loop Sagnac interferometer as first described in Ref. [33]. Following the main components shown in Fig. S4, two linearly polarized counterpropagating beams comprising the interferometer are isolated along the fast and slow axes of ~ 10 m of polarization-maintaining fiber and are modulated in phase with a frequency that matches the transit time of light through the interferometer. The linearly polarized light traveling along each of these paths passes through a quarter-waveplate and is converted into circularly polarized light just above the sample. In the absence of magnetic field, the apparatus is completely reciprocal by symmetry except for the sample. Thus, upon reflection, one branch of the interferometer acquires a phase shift of $+\theta_K$, while its orthogonally polarized counterpart acquires an opposite phase shift of $-\theta_K$. The two phase shifts are added at the detector and extracted from the ratio of the first and second harmonics of the modulated signal.

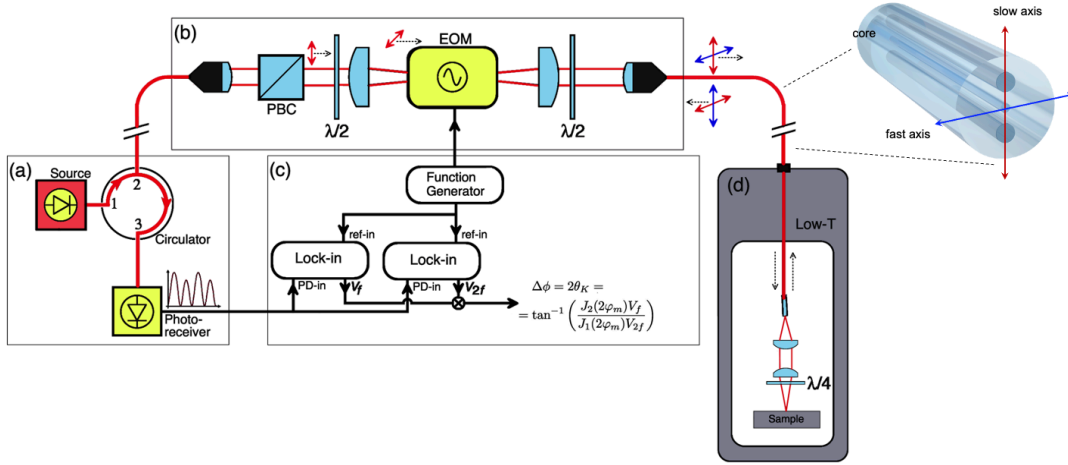


FIG. S4: Schematic of the zero-area loop Sagnac interferometer used in this study. On the right is the end-part showing one beam that enters the quarter waveplate from the fast axis as right circularly polarized, and reflected back into the slow axis as left circularly polarized after experiencing a Kerr angle shift. A second beam propagates in the direction of the sample in the slow axis and is reflected into the fast axis.

S6. AB-INITIO CALCULATIONS OF THE SURFACE BAND STRUCTURE OF LUPTBI

Ab initio calculations were performed within the density-functional theory framework with the generalized gradient approximation, which is implemented into the VASP package [54]. A 54-atomic-layer-thick slab model was employed to simulate the LuPtBisurface, in which the top surface is terminated by Bi and the bottom surface is by Lu. A vacuum layer with more than 50 Å thick is employed in the z -direction to avoid inter-slab interactions. A grid of 12×12 is used for the 2D Brillouin zone integration. Spin-orbit coupling was included in all calculations.

In particular, the Bi-termination surface is shown in Fig. S5, exhibiting a van-Hove singularity (VHS) at $E = -0.10$ eV near the M-point, about 5% offset along the line from M to Γ . 6 such VHS points appear in the first Brillouin zone.

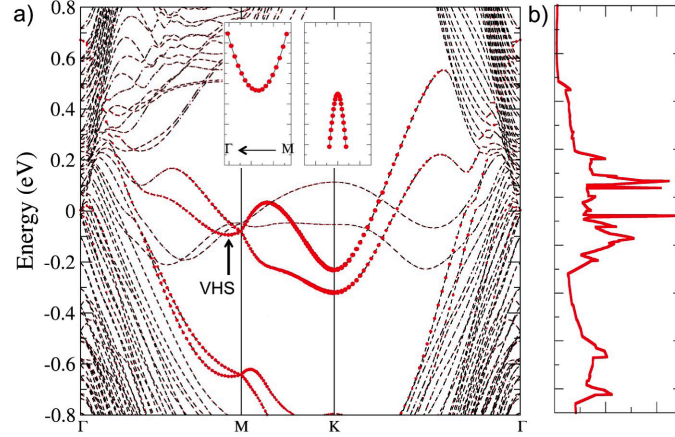


FIG. S5: The surface band structure and density of states (DOS) from ab-initio calculations. (a) Band structure. The size of red circles represents the projection to the surface Bi atom on the top surface. (b) DOS projected to the surface Bi states. The Fermi energy is shifted to zero. A Van Hove singularity (VHS) point exists in the surface band near the M point (nearly 10% position from M to Γ), corresponding to DOS singularity at about -0.1 eV. Two insets are shown to demonstrate the VHS point, in which the left inset shows the up-opening parabolic dispersion along the $\Gamma - M$ line while the right inset shows the down-opening parabolic dispersion along the line perpendicular to the $\Gamma - M$ direction. The saddle (VHS) point is highlighted by blue arrows.